Kinesin Has Three Nucleotide-dependent Conformations

IMPLICATIONS FOR STRAIN-DEPENDENT RELEASE*

Jun Xing‡, Willy Wriggers§, Geraldine M. Jefferson¶, Richard Stein‖, Herbert C. Cheung‡, and Steven S. Rosenfeld¶**

From the Departments of ‡Biochemistry and Molecular Genetics and ¶Neurology and the ‖Graduate Program in Cell and Molecular Biology, University of Alabama at Birmingham, Birmingham, Alabama 35294 and the §Department of Molecular Biology, Scripps Research Institute, La Jolla, California 92037

Although crystallographic information is available on several nucleotide-induced states in myosin, little is known about the corresponding structural changes in kinesin, since a crystallographic model is only available for the kinesin:ADP complex. This makes it difficult to characterize at a molecular level the structural changes that occur in this motor through the course of its ATPase cycle. In this study, we report on the production of a series of single tryptophan mutants of a monomeric human kinesin motor domain, which demonstrate nucleotide-dependent changes in microtubule affinity that are similar to wild type. We have used these mutations to measure intramolecular distances in both strong and weak binding states, using florescence resonance energy transfer. This work provides direct evidence that movement of the switch II loop and helix are essential to mediate communication between the catalytic and microtubule binding sites, evidence that is supported as well by molecular modeling. Kinetic studies of fluorescent nucleotide binding to these mutants are consistent with these distance changes, and demonstrate as well that binding of ADP produces two structural transitions, neither of which are identical to that produced by the binding of ATP. This study provides a basis for understanding current structural models of the kinesin mechanochemical cycle.

A thorough understanding of the mechanism of action of molecular motors requires molecular-level detail on the structures of the intermediates in the motor's chemomechanical cycle. Such information is now available through the use of crystallographic models of the molecular motor myosin in various nucleotide states, and this has provided direct evidence that small conformational changes induced by nucleotide hydrolysis and product release are amplified by a segment that connects the motor and regulatory domains (1), and that drives translational movement of the latter (2). A similar level of understanding of the mechanism of the motor kinesin is not available, since crystallographic information is only available in the ADP-bound state (3, 4). Nevertheless, a variety of methods have been used to examine the structural transitions that this motor undergoes through its ATPase cycle. Fluorescence anisotropy decay studies of labeled kinesin dimer constructs, for example, demonstrated the presence of a hinge connecting the motor domains to the tail, whose flexibility varied with the nucleotide present in the active site (5). Likewise, image reconstructions of kinesin-decorated microtubules were interpreted to show a nucleotide-dependent change in orientation in the kinesin motor domain when attached to a microtubule (6).

A combination of spectroscopic and imaging techniques have more recently been used to address the nature of the conformational changes that kinesin undergoes in its ATPase cycle (7). Both spin resonance and fluorescence resonance energy transfer studies of single cysteine mutants of the motor domain demonstrated conformational differences between nucleotide-free and AMPPNP[1]-saturated kinesin motor domains, but only when the kinesin motor domain was bound to microtubules. Image reconstructions of cryoelectron micrographs of gold-labeled kinesin constructs also demonstrated a change in the orientation of the carboxyl terminus. However, EM studies also revealed that, although the carboxyl terminus of microtubule-bound kinesin:AMPPNP or kinesin:ADP:AlF$_4$ assumed a single orientation, that for either nucleotide-free kinesin or kinesin:ADP could assume one of two discrete orientations while bound to the microtubule. If the equilibrium constant between these two states were to have a large temperature dependence, the free energy for this transition could provide additional force or movement. Thus, structural models of the kinesin mechanochemical cycle need to be consistent with information on the number of nucleotide-dependent kinesin states and on the equilibrium and rate constants that connect them.

In this study, we have addressed this issue by generating a series of single tryptophan mutants of human kinesin. We have measured intramolecular distances between these tryptophan residues and a fluorophore in the catalytic site in various kinesin:nucleotide states, by using fluorescence resonance energy transfer (FRET). Results of FRET studies are consistent with kinetic studies of nucleotide binding to these mutant kinesins, and demonstrate that kinesin can assume three discrete conformations. The relevance of these conformations to models of strain-dependent release and processivity will be discussed.

** To whom correspondence and reprint requests should be addressed: Dept. of Neurology, University of Alabama at Birmingham, UAB Station, Birmingham, AL 35294. Tel.: 205-934-1432; Fax: 205-975-7546; E-mail: srosenfeld@email.neuro.uab.edu.

[1] The abbreviations used are: AMPPNP, adenosine 5′-(β,γ-imino)-triphosphate; 2′dmD, 2′-deoxy-mant-ADP; 2′dmT, 2′-deoxy-mant-ATP; FRET, fluorescence resonance energy transfer; K332, human kinesin construct containing the monomeric motor domain, and consisting of the first 332 amino-terminal residues; mant, *N*-methylanthranyloyl; MDCC, 7-diethylamino-3-((((2-maleimidyl)ethyl)amino)carbonyl)coumarin.

EXPERIMENTAL PROCEDURES

Materials—Oligonucleotide primers used in the mutagenesis were synthesized by Life Technologies, Inc. The QuikChange site-directed mutagenesis kit was obtained from Stratagene, Inc. (La Jolla, Ca.). Media components were obtained from Difco Laboratories (Detroit, MI). Protease inhibitors, isopropyl-β-D-thiogalactopyranoside, and reagents for buffers and agarose gel electrophoresis were obtained from Sigma. Ribonuclease A and deoxyribonuclease I were purchased from Roche Molecular Biochemicals. Pre-packed Sephadex G25 columns were purchased from Amersham Pharmacia Biotech. Nickel-nitrilotriacetic acid-agarose was obtained from Qiagen (Chatsworth, CA). Chemicals used for SDS-polyacrylamide gel electrophoresis were from Bio-Rad. Centriprep-10 concentrators were purchased from Amicon, Inc. (Cherry Hill, NJ).

Site-directed Mutagenesis and Kinesin Preparation—Mutagenesis was carried out by using a clone of human kinesin kindly provided by Dr. Ron Vale (University of California, San Francisco, CA). Mutagenesis was performed according to the QuikChange kit protocol, and mutations were verified by DNA sequencing. The mutated plasmid was transformed into XL1-Blue *Escherichia coli*. Transformants were selected on plates of LB with 100 μg/ml ampicillin. The mutants were analyzed by agarose electrophoresis and sequenced. Positive DNA was transformed into *E. coli* BL21(DE3) for expression of each mutant. Transformants were selected on plates of LB with 100 μg/ml ampicillin. For purification of Val-238, Ala-260, Phe-318, and Val-329, 12 liters of culture were grown at 30 °C and 250 rpm in LB with 200 μg/ml ampicillin for 48 h. For preparation of Tyr-228, cultures were grown at 37 °C and induced for 3 h by the addition of isopropyl-β-D-thiogalactopyranoside to 1 mM. Cells were harvested by centrifugation and stored at −70 °C.

For preparation of the kinesin mutant proteins, the frozen cells were thawed and resuspended in 3 ml of cold Lysis Buffer (50 mM Tris, pH 7.9, 10% sucrose, 0.3 M NaCl, 5 mM MgCl$_2$, 0.5 mM ADP, 1 mM phenylmethylsulfonyl fluoride, 2 μg/ml leupeptin, 1 μg/ml pepstatin A, 2 μg/ml aprotinin)/g of cells. Lysozyme was added to 1 mg/ml, and the suspension was kept cold on ice for 30 min with occasional mixing. The sample was sonicated, ribonuclease A was added to 10 μg/ml, deoxyribonuclease I was added to 5 μg/ml, and the suspension was incubated on ice for 15 min, followed by centrifugation at 15,000 × g for 20 min. The clarified sample was filtered and added to 12 ml of a 1:1 suspension of nickel-nitrilotriacetic acid-agarose pre-equilibrated in Lysis Buffer. The sample was nutated at 4 °C for 2 h. The resin was pelleted and loaded into a 0.5 × 3-cm column at 4 °C. The column was washed for 2 h at 0.6 ml/min with Wash Buffer (20 mM Tris, pH 7.9, 0.5 mM NaCl, 5 mM MgCl$_2$, 0.5 mM ADP, 1 mM phenylmethylsulfonyl fluoride). The kinesin was eluted with a gradient of 40–500 mM imidazole in Wash Buffer.

Microtubule ATPase and Binding Assays—The microtubule activated ATPase activity of kinesin constructs was measured by mixing 20–30 nM kinesin with a greater than 20-fold molar excess of taxol-stabilized microtubules in 20 mM HEPES, 50 mM potassium acetate, 5 mM MgCl$_2$, 1 mM dithiothreitol, 0.1% bovine serum albumin, 2 mM ATP, pH 7.20. ATP hydrolysis was monitored by the oxidation of NADH in an enzyme-linked assay, as described (8). Binding affinities of kinesin constructs in the presence of ADP ± aluminum fluoride were determined by an centrifugation assay, as described (9).

Kinetic Measurements—Rates of binding of 2′-deoxy-mant-ATP and 3′-deoxy-mant-ATP to nucleotide-free kinesin constructs were made in a Hi-Tech stopped flow spectrometer with instrument dead time of 1.6 ms. Kinesin samples were made nucleotide-free immediately prior to the experiment with apyrase, as described (10). Binding of nucleotide was monitored by energy transfer, using an input monochromator to generate an excitation wavelength of 295 nm and a 400-nm long pass filter for the output, as described in prior studies (11, 18).

For studies of phosphate release rates, kinesin samples were made nucleotide-free with apyrase, as described (10), and mixed in one syringe of the stopped flow with a 2-fold molar excess of MDCC-labeled phosphate-binding protein. Varying concentrations of ATP were placed in the other syringe, and both syringes contained 100 μM 7 methylguanosine, 0.5 unit/ml purine nucleoside phosphorylase. The rate of phosphate binding to the MDCC-labeled phosphate binding protein was measured by setting the excitation monochromator to 425 nm and by using a 450-nm long pass filter over the output photomultiplier. The absorbance profile of the 450-nm output filter demonstrated negligible transmission at the exciting wavelength.

Time-resolved Fluorescence Measurements—Complexes of 2′-deoxy-mant-ADP ± aluminum fluoride with kinesin mutants were made as

described previously (9). The fractional binding of the mant nucleotide to kinesin was determined by equilibrium filtration through Centricon tubes (Amicon). This information was used to correct for the less than complete labeling of construct with fluorescent nucleotide. In fact, labeling ratios were in the range of 0.84–0.96 for the various constructs. Complexes of 2′-deoxy-mant-ADP with aluminum fluoride were prepared as described previously (9). In brief, a 10-fold molar excess of 2′-deoxy-mant-ADP was added to each construct, and allowed to bind for 20 min at 4 °C. AlNO$_3$ was added to 1 mM, NaF was added to 5 mM, and the complex was allowed to equilibrate at room temperature for an additional 20 min. Excess nucleotide was removed by gel filtration on pre-poured Sephadex G25 columns (PD10, Amersham Pharmacia Biotech).

All fluorescence measurements were made at 20 ± 0.1 °C. Steady state emission spectra were recorded on an ISS PCI photon-counting spectrophotometer. These spectra were corrected for variation of the detector system with wavelength. Quantum yields of tryptophan residues were determined with the comparative method, as described (12). Fluorescence intensity decay of tryptophan was measured in the time domain with an IBH 5000 photon-counting lifetime system equipped with a very stable flash lamp operated at 40 kHz in 0.5 atmosphere of hydrogen. For FRET studies, the intensity decay data of the donor tryptophan collected from donor-alone and donor-acceptor samples were used to calculate the distribution of interprobe distances as described previously (12, 13). The distributions of the distances were calculated using the program CFS_LS/GAUDIS, assuming the probability distribution to be a Gaussian function. The distance distribution is characterized by two parameters: the mean distance R and the half-width of the distribution. The value of the half-width is related to the standard deviation of the distribution (σ) by the relationship: half-width = 2.354σ. The Forster critical distance R_o was determined for each donor-acceptor pair and for both strong and weak binding states. Because the two recovered distance parameters, R and the half-width, are highly correlated, the goodness-of-fit values of χ_R^2 depend on the entire set of parameters, not just a single one (14). An additional problem is that the variance space is usually non-linear. The joint confidence intervals for a given determined parameter can be judged by examining the χ_R^2 surfaces calculated by the support plane procedure (14). These surfaces were calculated for the mean distance and half-width as has been done in previous analyses of distance distributions (12, 13, 15).

Simulations of Kinesin Mutant Structure—The simulations were carried out with the program X-PLOR (36) using the CHARMM force field (37), version 24, and simulation parameters as described (29). 2′-Deoxy-mant-ADP and ATP were parametrized by combining standard CHARMM parameters and atomic charges for the nucleotides with those of phenylalanine, methylated COOH terminus from methyl acetate, and *N*-methylamide COOH terminus (for the fluorophore). The stereochemistry of the resulting model was validated by energy-minimization and visual inspection. The force field for 2′-deoxy-mant-ADP and ATP is available from the authors.

We modeled mant-ADP and mant-ATP kinesin starting from the ADP crystal structure of rat kinesin (4), including the crystallographic water molecules. The triphosphate of the nucleotide for the ATP case was constructed based on our earlier model (29). In addition to the modification of the nucleotide, side chains corresponding to the five tryptophan mutants (human kinesin numbering: 228, 238, 260, 318, 329) were replaced with tryptophan side chains (rat kinesin numbering: 229, 239, 261, 320, 331). To account for the effect of surface water, kinesin was immersed in a shell of explicit water molecules of 6-Å thickness, which corresponds to approximately two layers of water molecules. The total size of solvated (mant) ADP-kinesin was 10,017 atoms (1545 water molecules), and the total size of solvated (mant) ATP-kinesin was 9,988 atoms (1534 water molecules).

The kinesin structures were refined by simulated annealing (29), using a maximum temperature of 500 K. After an initial energy minimization, the systems were heated up to 500 K in steps of 10 K by Langevin dynamics (36, 38) over a 50-ps time period, using a uniform friction constant of 50 ps^{-1} for heavy atoms and 0 for hydrogen atoms. The temperature was held constant (at 500 K) from 50 to 80 ps. Subsequently the systems were cooled down from in steps of 1.5 K over a 200-ps time period. The annealing was stopped at the low temperature of 200 K, which quenched the mobility of the cooled system. The final structures were energy-minimized after a total of 280 ps of simulation.

We employed distance constraints in certain simulated systems to stabilize desired conformations or to induce desired conformational transitions. First, the nucleotide sugar and base were anchored to the protein by constraining six atom pair distances to their crystallographic

TABLE I

Dissociation constants for microtubule:kinesin binding in ADP $\pm$ AlF$_4$

Conditions: 20 mM HEPES, 50 mM potassium acetate, 5 mM MgCl$_2$, 1 mM dithiothreitol, 0.1% bovine serum albumin, 4 mM ATP, pH 7.20. Values are $\pm$ 1 standard deviation. $K_{D(ADP)}$, dissociation constant for microtubule binding in the presence of 1 mM ADP. $K_{D(ADP+AlF4)}$, dissociation constant for microtubule binding in the presence of 1 mM ADP, 1 mM AlNO$_3$, and 5 mM NaF. Values are $\pm$ 1 standard deviation.

Mutant	Location	$K_{D(ADP)}$	$K_{D(ADP+AlF4)}$
		μM	μM
Wild type		22.4 ± 3.7	1.4 ± 0.2
Y228W	$\beta 7$	26.1 ± 6.8	0.8 ± 0.1
V238W	L11	$>100^a$	2.0 ± 0.6
A260W	$\alpha 4$	73.0 ± 32.8	1.0 ± 0.3
F318W	$\alpha 6$	38.6 ± 5.1	0.4 ± 0.1
V329W	Neck linker	23.5 ± 4.9	0.2 ± 0.1

[a] Less than 10% occupancy at 100 μM tubulin was observed, making accurate measures of K_D impossible for this construct.

values using a Hookean potential (force constant 5.0 kcal mol^{-1} Å^{-2}): N6-CZ$_{14}$, N7-CA$_{91}$, C2-NE2$_{94}$, C2-CB$_{16}$, C5′-CB$_{16}$, C5′-CG$_{94}$ (following Protein Data Bank nomenclature; the first atom refers to the nucleotide, and the second, including the subscript residue number, refers to the protein). This procedure was necessary to prevent a detachment of the nucleotide after invoking FRET-based distance constraints. The phosphate and fluorophore were allowed to move freely. Also, as described elsewhere (29), we enforced the proper coordination of the γ-phosphate in ATP-kinesin by constraining the distance between the γ-phosphorus and the α-carbon of rat Gly-235 (= human Gly-234) to 3.9 Å using a Hookean potential (force constant 5.0 kcal mol^{-1}Å^{-2}). Finally, FRET distance constraints were enforced in certain simulated annealing simulations between the centroids of the resonant side chains of the tryptophan residues and those of the mant fluorophore. The constraints were enforced using XPLOR NOE constraints (37), ramped linearly from zero to their maximum value of 5.0 kcal mol^{-1} Å^{-2} during 30–80 ps of simulation time, and subsequently held constant during the 80–280-ps cooling period. In this work we present results of enforcing a single constraint at residue 239 in the human kinesin sequence (39).

RESULTS

Steady State Binding and Enzymatic Properties of Kinesin Mutants—The motor domain of wild type human kinesin is devoid of tryptophans. We have taken advantage of this by generating five mutants with trytophan substituting for Tyr-228, Val-238, Ala-260, Phe-318, and Val-329. These residues are located in $\beta 7$, L11, $\alpha 4$, $\alpha 6$, and the neck linker, as defined by the crystal structure of kinesin:ADP (3, 4). Each mutant was cloned into the pET 21D vector, generating a protein consisting of the 332 amino-terminal residues of human kinesin, which constitute the motor domain, followed by a hexahistidine sequence for affinity purification (9). Hence, each mutant contains only one tryptophan residue, located in the above-defined positions. These mutants were generated in order to look at changes in FRET efficiencies as a function of microtubule binding state. The microtubule affinity of kinesin is modulated by the nucleotide occupying its catalytic site, with ADP generating a "weak" binding conformation and ATP generating a "strong" binding conformation (9, 16). In order to ensure that these mutants are still capable of demonstrating a strong-to-weak transition, we measured binding of these mutant kinesin constructs to microtubules by a cosedimentation assay, as described previously (9). Binding was measured in the presence of 1 mM ADP, to generate a weak binding state, and in the presence of 1 mM ADP, 1 mM AlNO$_3$, and 5 mM NaF, to produce a strong binding state (9, 10). As Table I demonstrates, Y228W, F318W, and V329W bind to microtubules in the presence of ADP with affinities similar to wild type, whereas the affinity of A260W is 3.5-fold lower. In the presence of 1 mM ADP, maximal binding for these constructs was 0.86–0.92. No appreciable binding of V238W could be demonstrated in the presence of 1 mM ADP. By contrast, addition of AlF$_4$ + ADP enhanced the

TABLE II

ATPase properties of kinesin mutants

Conditions were as described in Table I. Values are $\pm$ 1 standard deviation.

Mutation	Location	k_{cat}	$K_{0.5(MT)}$	$k_{cat}/K_{0.5(MT)}$
		s^{-1}	μM	$\mu M^{-1} \cdot s^{-1}$
Wild type		43.6 ± 7.8	26.0 ± 5.8	1.70
Y228W	$\beta 7$	24.1 ± 3.0	28.5 ± 6.0	0.85
V238W	L11	$>1.0^a$	$\gg 30^a$	
A260W	$\alpha 4$	7.0 ± 2.1	41.2 ± 17.5	0.17
F318W	$\alpha 6$	29.6 ± 9.2	26.4 ± 12.1	1.12
V329W	Neck linker	9.4 ± 0.7	4.3 ± 0.6	2.18

[a] Maximum ATPase rates of ≈ 1.0 s^{-1} were seen at 30 μM tubulin, without evidence of saturation of the ATPase rate, and making measures of k_{cat} and $K_{0.5(MT)}$ unreliable.

affinities of each construct, including V238W to values similar to wild type. In the presence of AlF$_4$ + ADP, maximal binding was 0.82–0.94 for these constructs. Mutation of Ala-260 and Val-238 to tryptophan appears to selectively reduce the microtubule affinity of kinesin:ADP, while having little effect on the affinity of the kinesin:ATP state. Nevertheless, the data in Table I demonstrates that each mutant is able to undergo a weak-to-strong conformational change, as evidenced by the marked increase in microtubule affinity induced by addition of aluminum fluoride.

The MgATPase activity of each mutant was measured (8) in the absence and presence of microtubules, and data were fitted to a hyperbolic dependence of rate on microtubule concentration. Table II summarizes the values of k_{cat}, $K_{0.5(MT)}$, and $k_{cat}/K_{0.5(MT)}$ for wild type K332 and for each of the single tryptophan mutants. Each of the mutants demonstrates a basal MgATPase activity, which varies from 0.03 ± 0.01 s^{-1} for F318W to 0.08 ± 0.04 s^{-1} for V238W, and compares to 0.03 ± 0.01 s^{-1} for wild type. Microtubule activation is minimal for V238W, reaching only 20-fold at 30 μM microtubules, and making measures of k_{cat} as well as $K_{0.5(MT)}$ highly unreliable. Our previous study (9) had demonstrated that the value of $K_{0.5(MT)}$ is a measure of the microtubule affinity of the predominant species under steady state conditions, which for wild type kinesin is an ADP-bound state. Values of $K_{0.5(MT)}$ for Y228W and F318W are also similar to wild type. For A260W, the binding affinity in the presence of ADP is consistent with the increase in $K_{0.5(MT)}$. In addition, the value of $k_{cat}/K_{0.5(MT)}$ is 10-fold lower than wild type, and suggests that there is a defect in the binding of the predominant steady state intermediate with microtubules. Similar results have been noted with S246F, a mutation in nearby L11 (34). By contrast, although k_{cat} and $K_{0.5(MT)}$ are lower in V329W, $k_{cat}/K_{0.5(MT)}$ is similar to wild type and suggests that the binding of the predominant nucleotide intermediate of this mutant to microtubules is normal.

Fluorescence Resonance Energy Transfer Distance Measurements—We have utilized the spectroscopic properties of these five single tryptophan mutants to measure intramolecular distances in strong and weak binding states using the technique of FRET (12, 13, 15). FRET distances were measured by determining the effect of a fluorescent ADP analogue (2′-deoxymant-ADP) in the catalytic site on the time-dependent fluorescence decay of the tryptophan residues. Table III summarizes values of the quantum yield (Q), overlap integral (J), and the Forster critical distance (R_o) for the five tryptophan-mant donor-acceptor pairs in the presence of ADP $\pm$ aluminum fluoride. As can be seen from the table, in the presence of ADP, four of the five tryptophan mutants have quantum yields lower than that for tryptophan in solution ($Q = 0.14$); and all of them are lower than 0.14 in the presence of ADP + AlF$_4$.

A donor-acceptor distance in a protein may not have a unique value because of protein dynamics. Instead, a more accurate

Single Tryptophan Mutants of Kinesin

TABLE III
Steady state tryptophan fluorescence properties of the five kinesin mutants

Conditions were as described in Table I. Q, tryptophan quantum yield in the absence of FRET acceptor; J, overlap integral between donor (tryptophan) emission and acceptor (mant) absorption spectra, in units of M^{-1} cm^{-1} nm^4; R_0, Forster critical transfer distance.

Mutant	ADP			ADP + AlF$_4$		
	Q	J	R_0	Q	J	R_0
		$\times 10^{15}$	Å		$\times 10^{15}$	Å
Y228W	0.173	0.0545	22.8	0.115	0.0559	21.4
V238W	0.079	0.1231	22.9	0.068	0.1229	22.3
A260W	0.074	0.1108	22.3	0.085	0.1117	22.8
F318W	0.021	0.1089	18.0	0.020	0.1140	18.0
V329W	0.052	0.0562	18.8	0.041	0.0555	18.0

TABLE IV
FRET distances and half-widths in kinesin in strong and weak states

R_{ADP}, FRET distance, in angstroms, between tryptophan residue and mant fluorophor of 2′-deoxy-mant-ADP. $R_{ADP+AlF4}$, FRET distance, in angstroms, between tryptophan residue and mant fluorophor of 2′-deoxy-mant-ADP in the presence of aluminum fluoride. Half-width (ADP), halfwidth of distance distribution between tryptophan and mant fluorophor for kinesin samples in the presence of 2′-deoxy-mant-ADP. Half-width (ADP + AlF$_4$): corresponding halfwidth in the presence of 2′-deoxy-mant-ADP + aluminum fluoride.

Residue	R_{ADP}	Half-width (ADP)	$R_{ADP+AlF4}$	Half-width (ADP + AlF$_4$)
	Å	Å	Å	Å
Y228W[a]	28.2	5.4	26.0	3.2
V238W	18.2	3.8	18.8	3.1
A260W	28.6	5.5	29.2	4.1
F318W[a]	18.4	3.2	17.2	3.5
V329W[a]	30.0	5.6	26.6	4.2

[a] Differences in R_{ADP} and $R_{ADP+AlF4}$ are significant for these mutants, using the criterion that the χ_R^2 surfaces of R for two distributions are sharp and intersect at χ_R^2 values above the 68% cutoff (see text for details).

approach is to describe the distance between donor and acceptor as a distribution of distances, with a mean distance, R, and a half-width of the distribution. The latter is thus a measure of the magnitude of the oscillation of the donor and acceptor around R. Table IV lists the values of R and half-widths for samples in the presence of 2′-deoxy-mant-ADP $\pm$ AlF$_4$. As Table IV demonstrates, the transition from the weak binding to the strong binding state is accompanied by distance changes that range from less than 1 Å to over 3.5 Å. Because of the strong correlation of the two parameters, R and the half-width, it is necessary to determine the range of mean distances consistent with the data by examining the χ_R^2 surfaces of the mean distances (14, 15). The range of mean distance is defined by the values of χ_R^2 in the χ_R^2 surface with random noise in 68% of repetitive measurements (one standard deviation). The calculated surfaces for R were sharp, as indicated by the narrow half-widths of the distributions. These surfaces for the half-widths were also sharp. If the χ_R^2 surfaces of R for two distributions are sharp and intersect at χ_R^2 values above the 68% cutoff, the distributions can be considered to be distinct (15). Using this criterion, we find differences in R between strong and weak binding states are significant for Y228W, F318W, and V329W. Likewise, the χ_R^2 surfaces of the half-widths are also sharp, indicating narrow ranges in the recovered values. Differences in half-width values between strong and weak binding states are significant for only V238W, A260W, and V329W.

Transient Kinetic Studies of 2′-Deoxy-mant-ATP Binding to Kinesin Mutants—In the FRET measurements discussed above, it has been assumed that the kinesin motor domain assumes an "ATP"-like conformation in the presence of 2′-deoxy-mant-ADP + aluminum fluoride. In order to confirm this, we have examined the kinetics of the 2′-deoxy-mant-ATP binding to each of the kinesin mutants, by monitoring mant fluorescence through energy transfer from the tryptophan residues. The distance changes summarized in Table IV, along with the values of R_o summarized in Table III, can together be used to predict changes that occur in the steady state emission of the mant fluorophore in the strong-to-weak transition. In particular, if 2′-deoxy-mant-ATP is mixed with nucleotide-free F318W in the stopped flow under conditions of energy transfer excitation, the resulting fluorescence transient should consist of two phases, reflecting changes in the tryptophan-mant distance during nucleotide hydrolysis. There should be an initial rising phase, due to binding of 2′-deoxy-mant-ATP to the active site, and the rate of this rising phase should demonstrate a hyperbolic dependence on nucleotide concentration. Hydrolysis of the bound 2′-deoxy-mant-ATP, however, will cause the tryptophan in position 318 to move away from the mant fluorophore by 1.2 Å, which would be associated with a decrease in the fluorescence emission intensity by 28%. Furthermore, the rate

of this falling phase should not demonstrate a nucleotide concentration dependence, and should match the rate of nucleotide hydrolysis and/or phosphate release. The fluorescence transient depicted in Fig. 1A demonstrates that this is the case. The fluorescence transient demonstrates both a rising and falling phase. The rate of the first phase demonstrates a hyperbolic dependence of rate on ligand concentration, whereas the second phase does not (Fig. 2A). Finally, the rate of the falling phase matches the rate of phosphate release, measured with MDCC-labeled phosphate-binding protein (Fig. 3A, Table V). In this experiment, a mixture of nucleotide-free F318W was mixed in the stopped flow with an excess of ATP, with an equal concentration of MDCC-labeled phosphate binding protein in each syringe. The rate of the initial fluorescence rise, indicating phosphate release in the first turnover, was plotted as a function of final ATP concentration. The data fit a hyperbolic dependence with a maximum rate of 5.2 s^{-1}, very close to the rate of the falling phase in Fig. 2A (7.6 s^{-1}).

Data in Table IV also predict that mixing Y228W with 2′-deoxy-mant-ATP should likewise produce a biphasic transient with the amplitude of the second, falling phase approximately 17% of the first, and with the rate constant of the first, rising phase also demonstrating a hyperbolic ligand concentration dependence. By contrast, a similar experiment with V238W would be predicted to produce only a single phase in the fluorescence transient, whose rate depends hyperbolically on ligand concentration. The fluorescence transients depicted in Fig. 1 (*B* and *C*), and the corresponding plots of rates *versus* [2′dmT] (Fig. 2, *B* and *C*) demonstrate that this is also the case. Furthermore, both constructs produce a phosphate release transient that has a rate similar to that for F318W (Fig. 3A). Mixing of nucleotide-free A260W with 2′-deoxy-mant-ATP produced results similar to that for V238W, whereas the corresponding experiment with Val-329 produced results similar to Y228W (data not shown).

The effect of microtubules on the phosphate release transient was also examined for Tyr-228, Val-238, Phe-318, and Val-329 by mixing 1 μM construct + 4 μM tubulin with ATP. In each case, the maximum rate of the fluorescence transient was at least 8–10-fold faster than the steady state rate, indicating phosphate release in the first turnover. Under saturating concentrations of ATP, the maximum rates of the transient were 39.2 ± 2.9 s^{-1} for Tyr-228, 9.9 ± 0.7 s^{-1} for Val-238, 22.9 ± 1.4 s^{-1} for Phe-318, and 72.6 ± 4.6 s^{-1} for Val-329 (Fig. 3B).

Transient Kinetic Studies of 2′-Deoxy-mant-ADP Binding to Kinesin Mutants—As shown above, monitoring of 2′-deoxy-
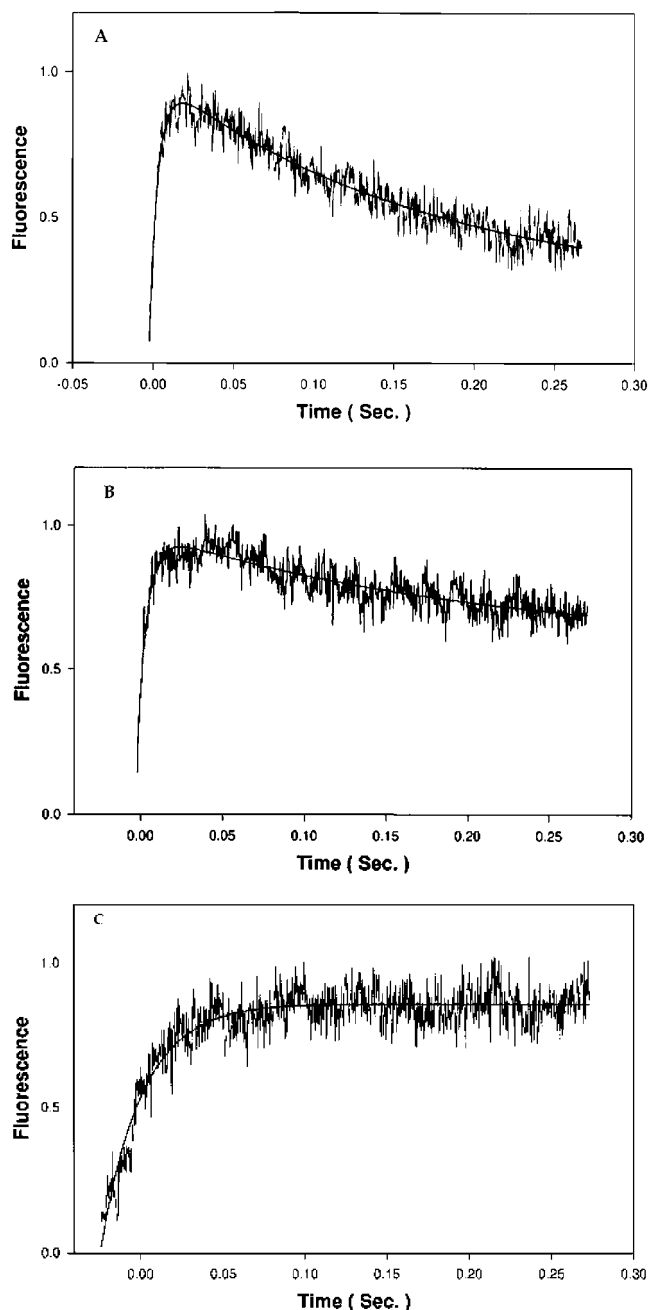
FIG. 1. **Fluorescence transient produced by mixing F318W (*A*), Y228W (*B*), and V238W (*C*) with 2′dmT and monitoring by energy transfer.** The *jagged curve* is the fluorescence tracing, and the *smooth curve* is a fit to two exponential processes (*A* and *B*) or one (*C*). For F318W (*A*) and Y228W (*B*), the fluorescence transient consists of a rising phase followed by a falling phase. By contrast, the transient for V238W (*C*) is monophasic.

mant-ATP binding to the single tryptophan constructs by energy transfer produces transients that are directly related to domain movements, and which vary in their nature depending on the construct studied. We therefore examined the kinetics of 2′-deoxy-mant-ADP binding to our constructs, monitored by energy transfer. Unlike the case for 2′-deoxy-mant-ATP, the resulting fluorescence transient for binding of 2′-deoxy-mant-ADP was found to consist of two phases of increasing fluorescence for each construct. Examples of such fluorescence transients are illustrated in Fig. 4*A* for V238W and Fig. 4*B* for F318W. In each case, the rate constant of the first phase varied with ligand concentration, whereas that for the second phase

showed minimal ligand concentration dependence (Fig. 5, *A* and *B*). For V238W, the rate of the faster phase demonstrated a clear hyperbolic dependence on ligand concentration, defining a maximum rate of $612 \ \mathrm{s}^{-1}$ (Fig. 5*A*). The deviation from a hyperbolic fit at the lowest ligand concentrations may be due to difficulty in extracting from the transient two rates that differ by a factor of only 2–4. By contrast, the other constructs showed a linear dependence of the rate of the first phase on ligand concentration, and a maximum rate could not be extrapolated. A representative plot is shown in Fig. 5*B* for F318W, and similar results were seen with Y228W, A260W, and V329W (data not shown). In each case, the final fluorescence intensity produced by mixing construct with 2′dmD was very similar to the final fluorescence intensity produced by mixing construct with 2′dmT. This is illustrated in Fig. 4*B*, which demonstrates convergence of the two fluorescence transients for the case of F318W mixed with either 2′dmT or 2′dmD. Table VI summarizes values of the apparent second order rate constant (k_a), the maximum rate (λ_1) for the first phase of the fluorescence transient, and the rate of the second phase (λ_2). The kinetics of 2′-deoxy-mant-ADP release from kinesin were also monitored by energy transfer, by mixing a complex of construct + 2-fold molar excess of of 2′-deoxy-mant-ADP with 2 mM ADP in the stopped flow. The resulting fluorescence transient fit a single exponential decay for each construct (Table VI).

Molecular Simulations of the Effect of the V238W Mutation on Kinesin Structure—Residue Val-238 is located in L11, adjacent to a portion of the kinesin molecule that is referred to as the switch II loop and helix (30). This region has been proposed to mediate communication between the catalytic site and the microtube binding domain. In particular, it has been suggested that this region undergoes a movement of several angstroms in response to nucleotide which would lead to a change in microtubule affinity (29, 32). Mutation of this position to tryptophan produces a kinesin construct that binds microtubules very weakly in the presence of ADP. This suggests that in this mutant, communication between the catalytic site and the microtubule binding domain is blocked. Our finding that the distance between position 238 and the catalytic site does not change in response to a change of microtubule affinity (Table IV) is consistent with this, and provides the first direct demonstration that movement of this region is necessary for normal motor function. We have expanded on this observation by performing molecular modeling of rat kinesin bound to mant-ADP and ATP, utilizing simulated annealing (29), coupled to FRET-derived distance constraints between the mant fluorophore and the side chain of residue Trp-239 (equivalent to position 238 in human kinesin).

As can be seen from Fig. 6*A*, kinesin exhibits significant nucleotide-dependent changes in the switch I (α3a/L9) and switch II (α4/L12) regions. These changes are induced by the closure of the nucleotide binding pocket through additional contacts with ATP that are mediated by the γ-phosphate-sensing residues: Ser-203 in switch I and Gly-235 in switch II (rat sequence). The direction and the magnitude (4.5 and 2.8 Å, for α3a/L9 and α4/L12, respectively) of the positional shifts agree very well with the results of earlier simulations of nucleotide-dependent effects in human kinesin (29), except for the magnitude of the α3a/L9 movement, which was smaller (2 Å) in the earlier model. The motions of the switch I region are a direct result of the placement of the adjacent γ-phosphate, whereas those of the distant α4/L12 microtubule binding site (35) are communicated and amplified by small shifts at the base of loop L11 toward the γ-phosphate. Although the movements of the two switch regions have been rendered separately in Fig. 6*A* for clarity, they are in fact coupled and are part of an allosteric mechanism that controls the shape of the microtubule binding
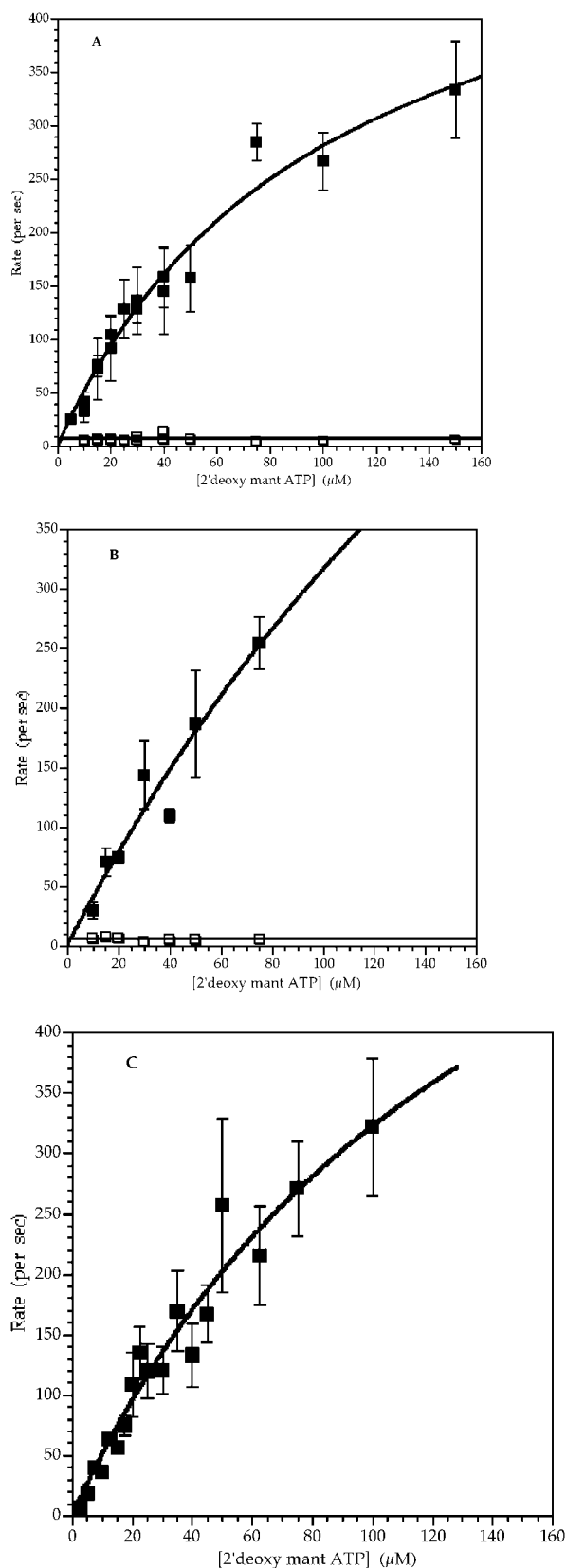
FIG. 2. **Rates of the two phases of the fluorescence transient produced by mixing F318W (*A*), Y228W (*B*), and V238W (*C*) with 2′dmT, plotted as a function of [2′dmT].** Conditions were as follows: 20 mM Hepes, 50 mM potassium acetate, 1 mM MgCl₂, 1 mM dithiothreitol, pH 7.2, 20 °C. For F318W (*A*) and Y228W (*B*), the rate of the rising phase demonstrates a hyperbolic ligand concentration dependence (*closed squares*), whereas the rate of the falling phase is independent of ligand concentration (*open squares*). By contrast, the transient for V238W (*C*) is monophasic, and the rate of this transient demonstrates
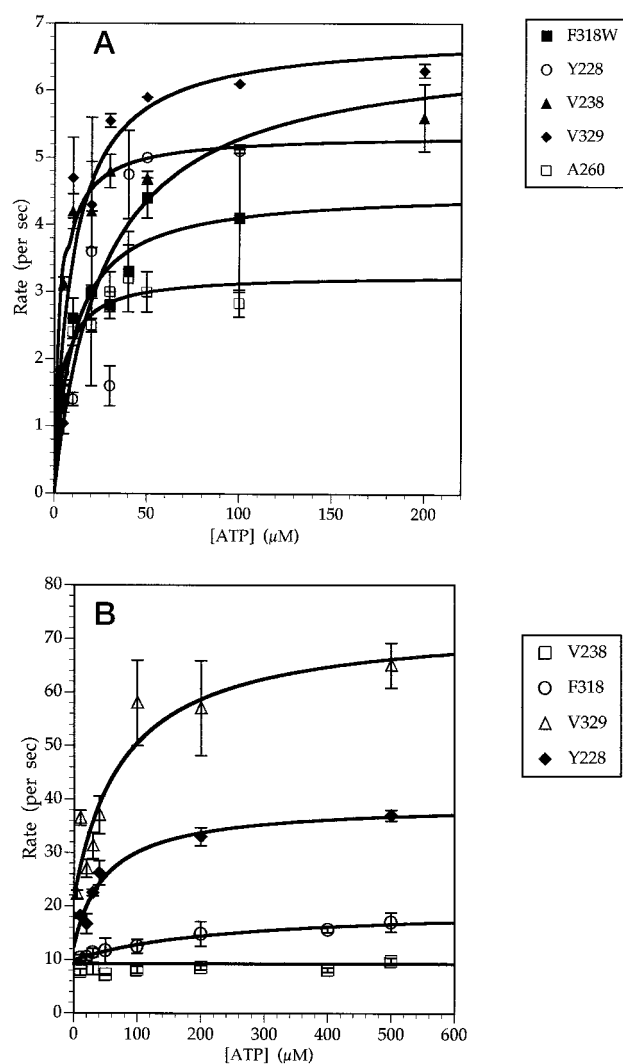

FIG. 3. *A*, rate of phosphate release from Y228W, V238W, A260W, F318W, and V329W plotted as a function of [ATP]. Phosphate release rates were measured by mixing kinesin construct + MDCC-labeled phosphate-binding protein with ATP in the stopped flow. Conditions were as in Fig. 1. Data were fitted to a series of hyperbolas, defining maximum rates of phosphate release of 6.8 s⁻¹ (Y228W), 5.6 s⁻¹ (V238W), 3.3 s⁻¹ (A260W), 5.2 s⁻¹ (F318W), and 7.0 s⁻¹ (V329W). Apparent binding constants derived from the hyperbolic fits range from 9.6 μM (V238W) to 26.5 μM (Y228W). *B*, rate of phosphate release from complexes of microtubule with Y228W, V238W, F318W, and V329W, plotted as a function of [ATP]. Conditions were as in *A*. Maximum rates of microtubule-activated phosphate release in the first turnover are 39.2 ± 2.9 s⁻¹ for Tyr-228, 9.9 ± 0.7 s⁻¹ for Val-238, 22.9 ± 1.4 s⁻¹ for Phe-318, and 72.6 ± 4.6 s⁻¹ for Val-329. Apparent binding constants range from 77 μM (V329W) to 244 μM (F318W), consistent with a reduction in nucleotide affinity induced by microtubule binding.
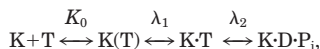
site (29), and presumably, microtubule affinity. Motions in the solvent-exposed loop L11 are not expected to be significant since this loop exhibited a purely thermal variability of 5 Å in the earlier simulations (29) and was disordered in the original human kinesin crystal structure (3).

The magnitude of the nucleotide-dependent movements seen in the switch I and switch II regions is significantly reduced when the FRET distances between the nucleotides and Trp-239 are enforced in the model (Fig. 6*B*). For both ATP and ADP kinesin, the FRET distance between Trp-239 and the mant

hyperbolic ligand concentration dependence. The hyperbolic concentration dependence of the rates define apparent second order rate constants and maximum rates summarized in Table V.

Data for binding of 2'-deoxy-mant-ATP to kinesin constructs were fitted to a rapid equilibrium binding step, followed by two sequential steps as follows,

$$K+T \overset{K_0}{\longleftrightarrow} K(T) \overset{\lambda_1}{\longleftrightarrow} K{\cdot}T \overset{\lambda_2}{\longleftrightarrow} K{\cdot}D{\cdot}P_i,$$

where T is ATP or 2'-deoxy-mant-ATP, K is the kinesin construct, D is ADP, and P_i is inorganic phosphate. The apparent second order rate constant for nucleotide binding is $k_a = K_0(\lambda_1)$, where λ_1 is the maximum rate of the first phase in the fluorescence transient, obtained by fitting the dependence of rate to a hyperbolic function. The rate of the second phase, when present, is defined as λ_2. It is compared to the rate of phosphate production (λ_{Phos}), monitored by mixing kinesin constructs + MDCC-labeled phosphate-binding protein with ATP. dmT, 2'-deoxy-mant-ATP.

Mutant	k_a	λ_1	λ_2	λ_{Phos}
	$\mu M \cdot s^{-1}$	s^{-1}	s^{-1}	
Y228W	4.9	844 ± 169	6.9 ± 1.5	5.7 ± 0.1
V238W	5.4	804 ± 241		5.6 ± 0.6
A260W	2.9	291 ± 47		3.3 ± 0.5
F318W	5.6	562 ± 144	7.6 ± 1.7	5.2 ± 0.1
U329W	5.0	279 ± 52	6.1 ± 1.9	7.0 ± 0.3

FIG. 5. **Rates of the two phases of the fluorescence transient produced by mixing V238W (*A*) and F318W (*B*) with 2'dmD, plotted as a function of [2'dmD].** Conditions were as in Fig. 2. For both constructs, the rate of the first phase demonstrates a ligand concentration dependence, which for V238W (*A*) varies hyperbolically, defining a maximum rate of 612 s^{-1}. For F318W (*B*), the rate of the first phase does not reach a maximum value over the ligand concentration range. For both constructs, the second phase shows little ligand concentration dependence of rate. The apparent second order rate constants defined by the dependence of rate on ligand concentration are summarized in Table VI.

$\alpha4$/L12 microtubule binding site by nearly 1 Å, due to the stabilization of the mediating loop L11. Finally, simulations reveal that the mant fluorophore appears to sterically restrain the nucleotide-dependent motions of the $\alpha3a$/L9 region, with the nucleotide-induced positional shift reduced by 1.7Å.

DISCUSSION

Crystallographic models of myosin in various nucleotide states have provided direct evidence that small conformational changes induced by nucleotide hydrolysis and product release are amplified by a segment which connects the motor and regulatory domains (1), and which drives translational movement of the latter (2). By contrast, the crystal structure of kinesin is available in only one state, in which ADP occupies the active site (3, 4), and structural models of the kinesin mechanochemical cycle have therefore been based on spectroscopic and image reconstruction data (5, 6). More recently, Rice *et al.* (7) examined the effect of nucleotide on intramolecular distance, segmental flexibility, and conformation. Nucleotide could modulate the mobility and energy transfer efficiency of spectroscopic probes attached to the carboxyl terminus of a
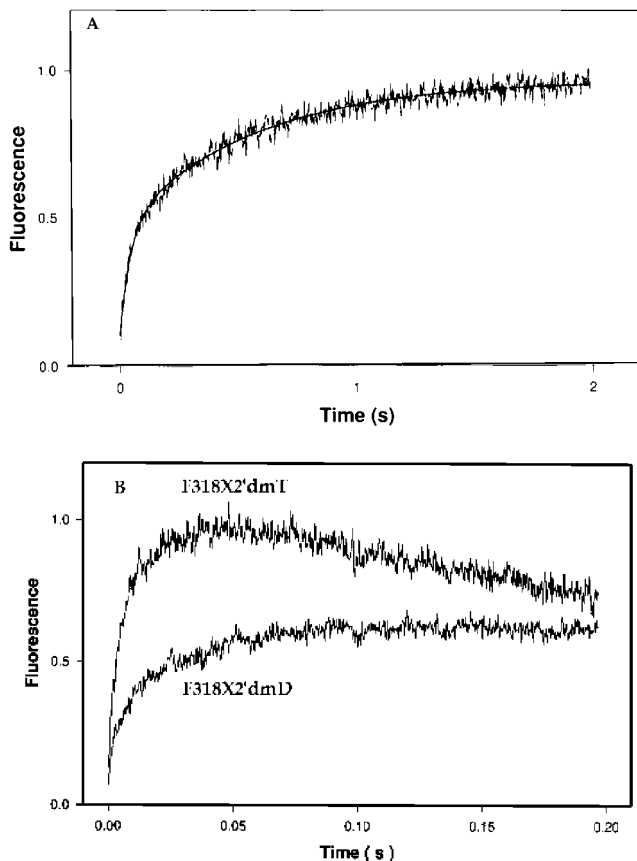

FIG. 4. **Fluorescence transients produced by mixing V238W (*A*) and F318W (*B*) with 2'dmD.** For both constructs, the transient consists of two phases of increasing intensity, unlike the case for mixing with 2'dmT (Fig. 1). In *panel B*, the transient for mixing F318W with 2'dmD is superimposed on that for mixing F318W with 2'dmT, and demonstrates that the final fluorescence level is the same in both cases.

fluorophore is about 10 Å smaller in the constrained model (Fig. 6*B*) compared with that in the unconstrained model. This produces a directional "pulling" of the fluorophore into a position pointing toward loop L11 (see *triangular* markers in Fig. 6, *A* and *B*). This in turn would reduce the movement of the
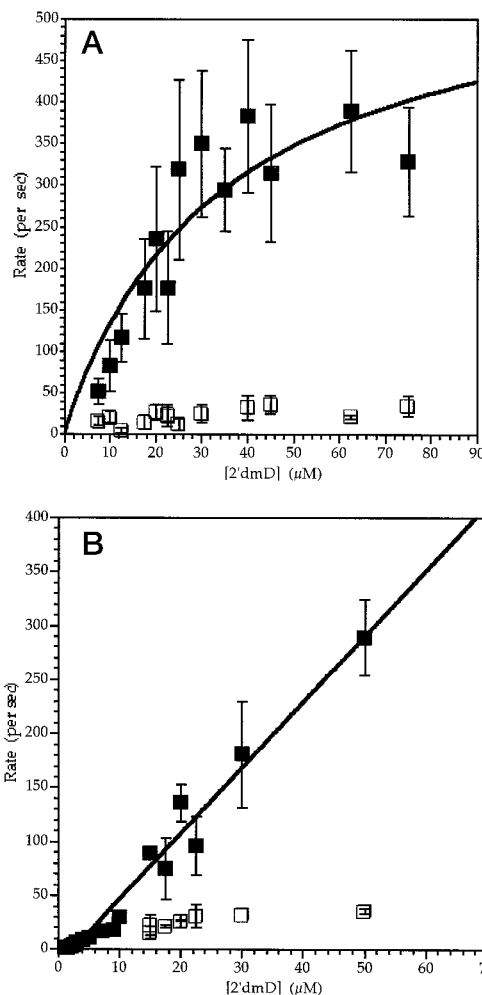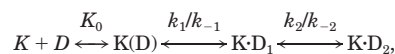
TABLE VI
Kinetic constants for binding and release of
2'-deoxy-mant-ADP to kinesin constructs

Data for binding of 2'-deoxy-mant-ADP was fitted to the following kinetic scheme,

$$K + D \underset{}{\overset{K_0}{\longleftrightarrow}} K(D) \underset{k_{-1}}{\overset{k_1}{\longleftrightarrow}} K \cdot D_1 \underset{k_{-2}}{\overset{k_2}{\longleftrightarrow}} K \cdot D_2,$$

where D is 2'-deoxy-mant-ADP and K is the kinesin construct. As in the case of ATP binding (Table V), the model predicts two phases in the fluorescence transient, where the rate of the first phase would vary with ligand concentration, and where $k_a = K_0 (\lambda_1)$. The rate of the second phase would be predicted to be independent of ligand concentration.

Binding reaction	k_a	λ_1	λ_2
	$\mu M \cdot s^{-1}$	s^{-1}	s^{-1}
Y228W × dmD	7.4	≫400	22.3 ± 6.1
V238W × dmD	31.2	612 ± 165	22.9 ± 9.0
A260W × dmD	16.1	≫400	18.6 ± 7.9
F318W × dmD	6.1	≫400	26.7 ± 6.5

Release reaction	λ
	s^{-1}
Y228W:dmD × ADP	0.02 ± 0.01
V238W:dmD × ADP	0.01 ± 0.002
F318W:dmD × ADP	0.06 ± 0.006
V238W:dmD × ADP	0.04 ± 0.008

monomeric kinesin construct, but only when the motor domain was bound to microtubules. This was taken to imply that microtubule binding is required for the nucleotide-induced structural changes in kinesin. Furthermore, cryo-electron microscopic images of microtubule-bound, labeled kinesin in the presence of various nucleotides demonstrated a single, unique orientation in the presence of AMPPNP or ADP+AlF$_4$ but two discrete orientations in the absence of nucleotide or in the presence of ADP. This was interpreted to suggest that kinesin:ADP was an equilibrium mixture of two states which are both appreciably populated at low temperatures.

However, our previous study demonstrated that even in the absence of microtubules, nucleotide could produce measurable changes in the structure of kinesin (5). We had demonstrated, utilizing fluorescence anisotropy decay, that nucleotide alone could alter the flexibility of a segment of the kinesin dimer that was located at the junction of the catalytic domain and the proximal tail, within the vicinity of the neck linker region. This led us to conclude that the strategic placement of intrinsic fluorescent probes in the kinesin motor domain might provide additional insight into the nature of the conformational changes that this motor undergoes during its mechanochemical cycle. Consequently, we generated five single tryptophan mutants of human kinesin, each with a tryptophan residue in
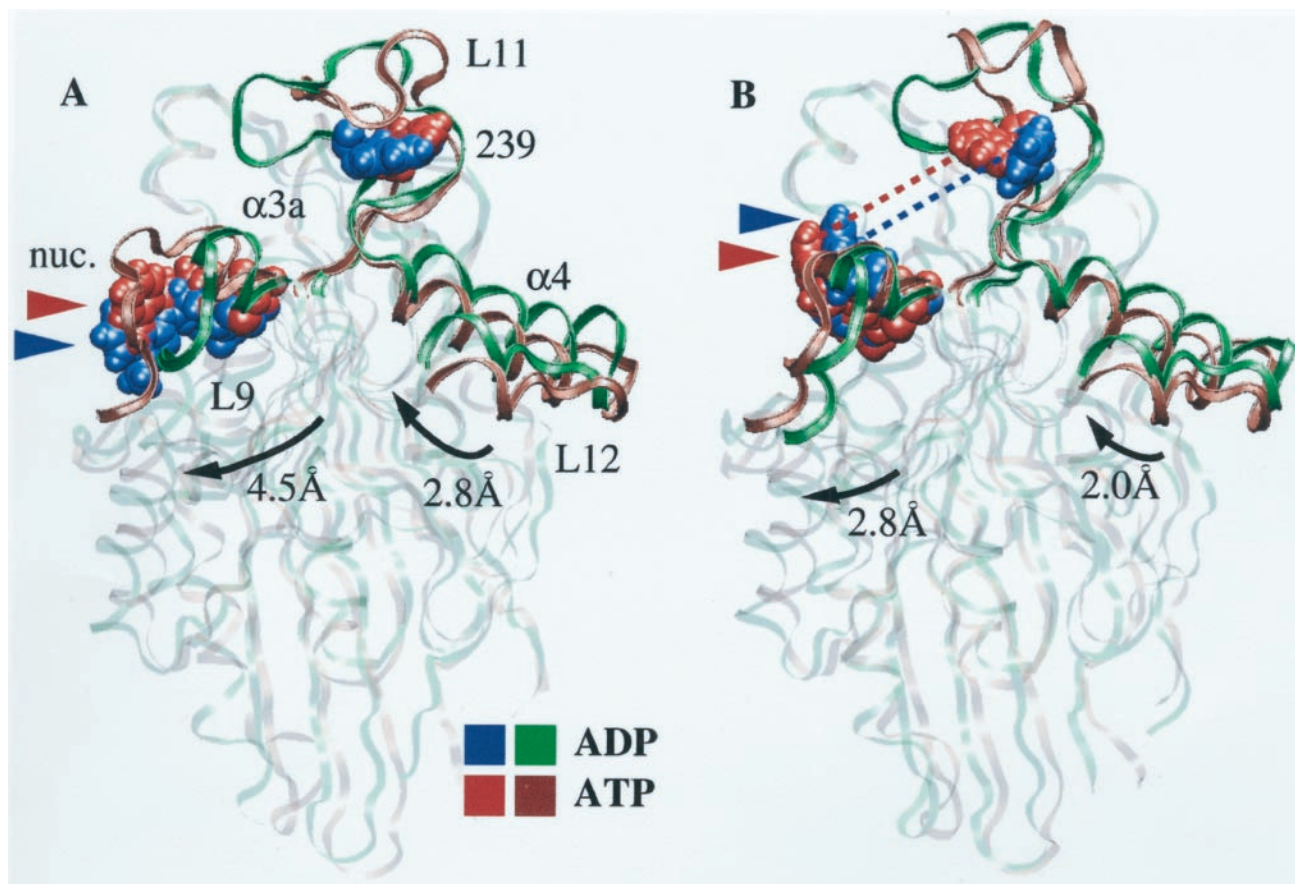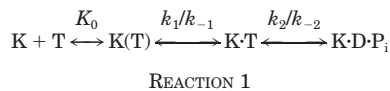

FIG. 6. **Computer modeling of the structural effect of the V238W distance constraint.** ATP-kinesin models (see "Experimental Procedures") are shown in *brown*, and ADP-kinesin models are in *green*. Rat Tp-239 (equivalent to position 238 in human kinesin) and the mant nucleotides are shown as van-der-Waals spheres in *red* (ATP cases) and *blue* (ADP cases). Triangles mark the position of the mant fluorophores bound to the nucleotides. The orientation of kinesin is equivalent to that in Fig. 11*B* in Ref. 29. Secondary structure elements (3, 4) involved in conformational changes are labeled in *panel A* and are shown in solid ribbon representation. The remainder of the protein is rendered transparent for clarity. *A*, control simulations of rat kinesin with mant nucleotides in the absence of the V238W distance constraint. The *two solid black arrows* illustrate nucleotide-dependent positional shifts exhibited by the α3a/L9 region (4.5 Å) and the α4/L12 region (2.8 Å). *B*, simulations of rat kinesin with mant nucleotides in the presence of FRET-derived distance constraints (*dashed lines*) between the mant fluorophore and the side chain of Trp-239. The *two solid black arrows* illustrate nucleotide-dependent positional shifts exhibited by the α3a/L9 region (2.8 Å) and the α4/L12 region (2.0 Å).

regions implicated in nucleotide or microtubule binding or in force transduction (3, 4). Each of these mutants demonstrated a weak-to-strong transition that was similar to wild type, as evidenced by the pronounced enhancement in microtubule affinity of the kinesin:ADP construct produced by addition of aluminum fluoride (Table I).
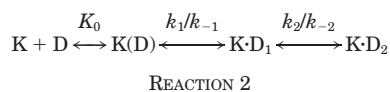
FRET measurements on these mutants were made to determine if changes in intramolecular distance occur with this weak-to-strong transition even in the absence of microtubules. As Table IV demonstrates, statistically significant intramolecular distance changes were seen in three locations as a consequence of the strong-to-weak transition: in Tyr-228, located in $\beta7$; in F318W, located in $\alpha6$; and in V329W, located in the neck linker. The largest change was seen in the neck linker region, consistent with previous measurements of microtubule-bound kinesin (7).

Our conclusion of residue movements during the strong-to-weak transition is based on small changes in the mean distances between tryptophan and the bound mant. These observed conformational changes predicted corresponding changes in the mant fluorescence emission when monitored by energy transfer in the stopped flow experiments. The energy transfer-generated kinetic results (Figs. 1 and 2) and the measured rate of phosphate release (Fig. 3A) unequivocally corroborated the FRET results. The generation of these mutants thus allows us to measure domain movements in real time that are directly related to the hydrolysis and/or phosphate release steps. They are also consistent with previous kinetic studies (19–21), which showed binding of ATP occurs via formation of an initial collisional complex, followed by an isomerization, with hydrolysis following these two transitions.

$$K + T \underset{}{\overset{K_0}{\longleftrightarrow}} K(T) \underset{k_{-1}}{\overset{k_1}{\longleftrightarrow}} K{\cdot}T \underset{k_{-2}}{\overset{k_2}{\longleftrightarrow}} K{\cdot}D{\cdot}P_i$$

REACTION 1

K is kinesin, T is ATP, K(T) is a collisional complex, P_i is inorganic phosphate, and K and k are equilibrium and rate constants, respectively. The apparent second order rate constant for the first fluorescent transition (k_a) is equal to $K_0 k_1$, assuming that k_{-1} is negligible, and the maximum rate is approximately k_1. Values of k_a and k_1 for the various constructs are similar to those previously measured for wild type K332 ($k_a = 9\ \mu M^{-1}\ s^{-1}$, $k_1 = 500\ s^{-1}$; Ref. 10). Likewise, the rate of the second phase in the transient (Fig. 2, A and B) is very similar to that produced by mixing wild type K332 with mant-ATP and monitoring through direct excitation (7 s^{-1}; Refs. 10 and 19).

When monitored by energy transfer, binding of 2′-deoxy-mant-ADP produced two transitions of increasing fluorescence for each construct, unlike the case for 2′dmT. The final fluorescence intensity when each construct was mixed with 2′dmD was essentially identical to that after mixing with 2′dmT, implying that the final conformations are the same. Kinetic data are consistent with the following model:

$$K + D \underset{}{\overset{K_0}{\longleftrightarrow}} K(D) \underset{k_{-1}}{\overset{k_1}{\longleftrightarrow}} K{\cdot}D_1 \underset{k_{-2}}{\overset{k_2}{\longleftrightarrow}} K{\cdot}D_2$$

REACTION 2

The two kinesin:ADP states are indicated by subscripts. The presence of a single phase in the 2′dmD release transient implies that K_2 is large, and that k_{-2} is rate-limiting in the release reaction.

The presence of two ADP states implies that there are three discrete kinesin:nucleotide conformations: one with ATP (mimicked by the complex with ADP + AlF_4), and two with ADP. Furthermore, if KD_1 and KD_2 differ in their microtubule affinities ("strong" and "weak," respectively), for purposes of this
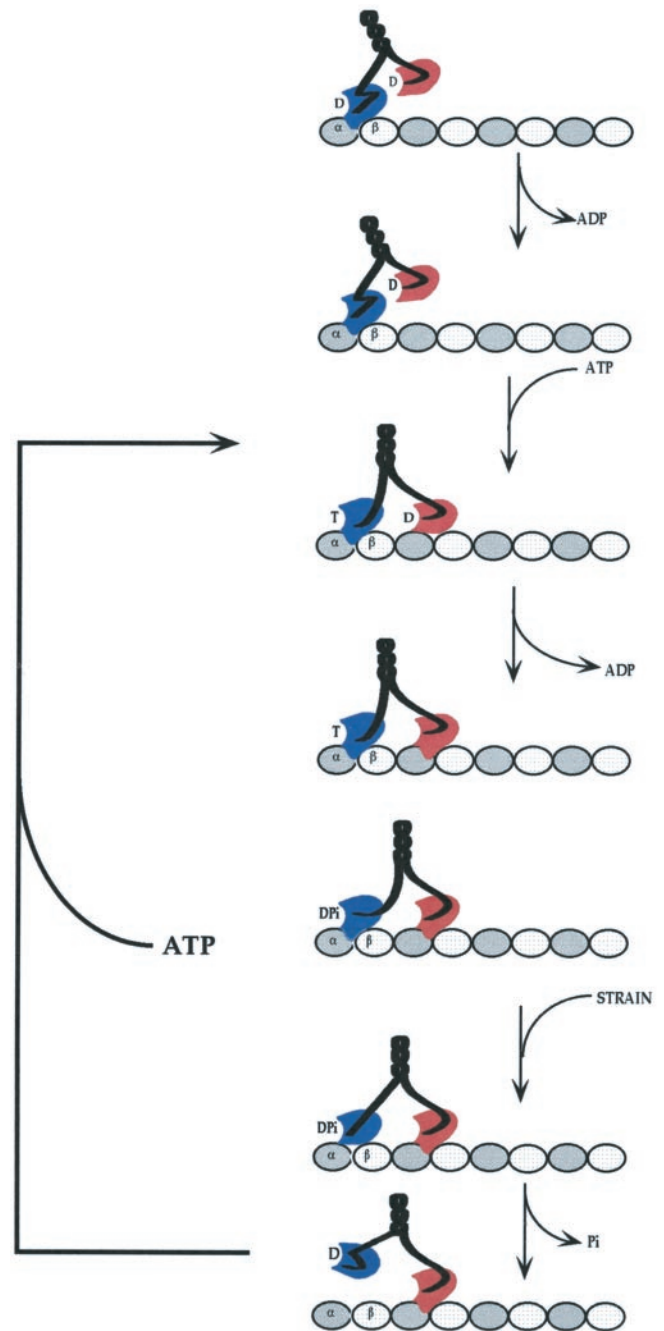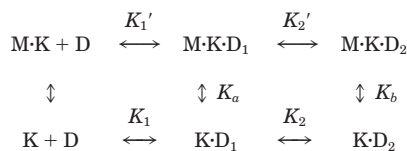

FIG. 7. **Model of strain-dependent release mechanism.** The role of strain in shifting a dynamic equilibrium is illustrated in this model. The cycle is entered with both heads of kinesin:ADP in a weak binding state. Weak attachment of the first (*blue*) head is followed by an isomerization and symbolized by the change in shape of the *blue* head, compared with the *red*. ADP rapidly dissociates, and its release is rapidly followed by binding of ATP. This is associated which change the orientation of $\alpha6$ and the neck linker region (*solid black line*), consistent with results from FRET studies (Table IV). The change in conformation produced by binding of ATP allows for weak binding of the second, ADP containing head (*red*). This is rapidly followed by its isomerization to a strong binding conformation, followed by ADP release. Hydrolysis of ATP by the first (*blue*) head follows. At this point, the head with ADP·P_i is proposed to be in a strong binding state, and that the rate-limiting step in this cycle is the conversion of this head to a weak binding conformation, leading to dissociation from the microtubule and release of phosphate. Strong binding by the second head (*red*) would introduce strain into the system, and this strain is proposed to accelerate the isomerization of strain into the system, and this strain is proposed to accelerate the isomerization of the first head into a weak binding ADP·P_i state. Release of phosphate would allow kinesin to re-enter the cycle, this time with the role of the two heads reversed.

discussion), then the affinity of kinesin:ADP for microtubules, as measured by steady state techniques, would depend not only on the microtubule affinities of KD_1 and KD_2, but also on the effect that microtubule binding has on their distribution. This is summarized in the following reaction pathway.

$$M{\cdot}K + D \overset{K_1{'}}{\longleftrightarrow} M{\cdot}K{\cdot}D_1 \overset{K_2{'}}{\longleftrightarrow} M{\cdot}K{\cdot}D_2$$

$$\updownarrow \qquad\qquad \updownarrow K_a \qquad\qquad \updownarrow K_b$$

$$K + D \overset{K_1}{\longleftrightarrow} K{\cdot}D_1 \overset{K_2}{\longleftrightarrow} K{\cdot}D_2$$

SCHEME 1

M stands for microtubule, and the other abbreviations are as defined above. If $K_a > K_b$ (*e.g.* KD_1 is strong binding), then $K_2{'} < K_2$, the MKD_1 state would be favored, and the microtubule affinity measured by steady state techniques would be greater than K_b. Conversely, if communication between the microtubule and nucleotide binding domains were blocked (*e.g.* $K_2 \approx K_2{'}$), then the measured kinesin:ADP affinity would approach K_b and would therefore be much lower. The low affinity of V238W:ADP for microtubules could thus be explained by a blocking of this microtubule-induced redistribution, and this in turn implies that this mutation uncouples communication between the catalytic site and the microtubule binding domain in the presence of ADP.

The existence of two kinesin:ADP states is directly relevant to models of processivity. A key feature of previous models is that the two heads of kinesin dimer are out-of-phase in their mechanochemical cycles, *e.g.* whereas one head is in a strong microtubule binding state, the other is in a weak state (23–25, 27). Our data, demonstrating a two-state equilibrium for kinesin:ADP, would be consistent with this if these two states were to differ in their microtubule affinity and if this two state equilibrium applied as well to kinesin:ADP:P_i. Prior to hydrolyzing its ATP, kinesin is in a single, strong binding conformation (9), characterized by the high fluorescence state seen with the single tryptophan mutants (Figs. 1A, B). Kinesin ADP:P_i ultimately relaxes into a weak binding, ADP conformation, coincident with phosphate release (Fig. 4*B*). This implies that, during the course of its ATPase cycle, kinesin ADP:P_I, like kinesin:ADP, transitions from a strong to a weak microtubule binding conformation. We propose that in the absence of applied strain from the second, attaching head, this transition would be slow or its equilibrium would be unfavorable, and phosphate and ADP release could occur before dissociation from the microtubule. This would explain the superstoichiometric phosphate burst for monomeric kinesin constructs, as described by Moyer *et al.* (26). Conversely, rapid attachment of the second, ADP containing head would place strain on the kinesin:ADP:P_i head, shifting its equilibrium to weak binding and producing coordinated dissociation.

The role of strain in shifting a dynamic equilibrium is illustrated in the model depicted in Fig. 7. We start the cycle with both heads of kinesin:ADP in a weak binding state-corresponding to KD_2 in the above scheme. Weak attachment of the first (*blue*) head is followed by an isomerization, corresponding to formation of KD_1 and symbolized by the change in shape of the *blue* head, compared with the *red*. ADP rapidly dissociates (≈300 s^{-1}; Ref. 26), and its release is rapidly followed by binding of ATP. This is associated with change in the orientation of $\alpha6$ and the neck linker region (*solid black line* in Fig. 7), consistent with our demonstration of the change in intramolecular distances of Phe-318 and Val-329 (Table IV). The change in conformation produced by binding of ATP allows for weak binding of the second, ADP containing head (*red* in Fig. 7). This is rapidly followed by isomerization of the ADP-containing head (*red* in the figure), as above, to a strong binding conformation, followed by ADP release. Hydrolysis of ATP by the first (*blue*) head follows. At this point, we propose that the head with ADP+P_i remains in a strong binding state, and that the rate-limiting step in this cycle is the conversion of this head to a weak binding conformation, leading to dissociation from the microtubule and release of phosphate. Strong binding by the second head (*red* in the figure) would introduce strain into the system, and we propose that this strain accelerates the isomerization of the first head into a weak binding ADP·P_i state. Release of phosphate would allow kinesin to re-enter the cycle, this time with the role of the two heads reversed, as has been previously pointed out by Moyer *et al.* (26).

This model also explains the effects of microtubules on the phosphate release transient (Fig. 3*B*). If V238W:ADP is "locked" in a weak binding conformation, then it follows that V238W:ADP:P_i is also locked in this conformation. Thus, with each ATPase cycle, this construct would dissociate from the microtubule once its bound ATP had been hydrolyzed. The rate-limiting step for this construct's ATPase cycle would be dissociation from the microtubule at 9.5 s^{-1} (k_4 in their Scheme I, Ref. 26), nearly identical to what we measure from the phosphate transient (Fig. 3*B*). The relatively slower phosphate release rate for F318W could reflect a much more subtle impairment in microtubule mediated communication, and may explain as well the slightly lower affinity that F318W:ADP has for microtubules (Table I).

Similarities in the crystal structures of kinesin and G proteins have led to the suggestion that position 238 in human kinesin is part of the switch II helix and loop, whose function is to mediate communication between the catalytic site and the microtubule binding domain (3, 30). Furthermore, comparisons of the crystal structures of human and rat kinesins, as well as of *Drosophila* ncd and yeast Kar3 have led to a model in which this region translates and rotates in response to nucleotide hydrolysis and phosphate release (3, 4, 30–32). A recent model, utilizing simulated annealing, also predicts that position 238 moves several angstroms in response to ATP hydrolysis and phosphate release (29). It follows that blocking the movement of position 238, as occurs in V238W (Table IV), should uncouple microtubule binding affinity from nucleotide state. The result would be a microtubule binding site that is completely "locked in" a weak binding conformation in the presence of ADP. However, the relatively normal affinity of V238W for microtubules in the presence of ADP+AlF_4 (Table I) suggests that movement of the switch II helix functions, at least in part, to mediate the interconversion of the two post-hydrolytic states, and emphasizes the importance of these two states in kinesin function.

We have utilized simulated annealing to see if this approach can explain how the V238W mutation might uncouple microtubule affinity from conformational changes in the catalytic site. The distance of the mutation site from the nucleotide observed in FRET experiments, when enforced in the simulation, suggests that the V238W mutant reduces the nucleotide-dependent variability of the switch II region and that of the $\alpha4$/L12 microtubule binding site. The inclusion of the FRET distance constraints provides a first model of the unknown conformation of the Val-238 mutant that explains its abnormal microtubule binding behavior. The modeling results lend further credibility to the hypothesis that the switch I and II regions communicate directly with each other and with the microtubule binding regions and suggest that computer simulations are capable of predicting the ATP state of kinesin in the absence of a crystal structure. Simulations involving con-

straints based on the other four tryptophan mutants presented in this work are currently under way that should shed light on the more distant conformational changes in the neck linker.

REFERENCES

1. Dominguez, R., Freyzon, Y., Trybus, K. M., and Cohen, C. (1998) *Cell* **94,** 559–571
2. Whitaker, M., Wilson-Kubalek, E. M., Smith, J. E., Faust, L., Milligan, R. A., and Sweeney, H. L. (1995) *Nature* **378,** 748–751
3. Kull, F. J., Sablin, E. P., Lau, R., Fletterick, R. J., and Vale, R. D. (1996) *Nature* **380,** 550–555
4. Sack, S., Muller, J., Marx, A., Thormahien, M., Mandelkow, E. M., Brady, S. T., and Mandelkow, E. (1997) *Biochemistry* **36,** 16155–16165
5. Rosenfeld, S. S., Correia, J. J., Xing, J., Rener, B., Dong, W., and Cheung, H. C. (1996) *J. Biol. Chem.* **271,** 30212–30222
6. Hirose, K., Lockhart, A., Cross, R. A., and Amos, L. A. (1995) *Nature* **376,** 277–279
7. Rice, S., Lin, A. W., Hart, C. L., Naber, N., Carragher, B. O., Cain, S. M., Pechatnikova, E., Wilson-Kubalek, E. M., Pate, E., Cooke, R., Taylor, E. W., Milligan, R. A., and Vale, R. D. (1999) *Nature* **402,** 778–784
8. Huang, T. G., and Hackney, D. D. (1994) *J. Biol. Chem.* **269,** 16493–16501
9. Rosenfeld, S. S., Rener, B., Correia, J. J., Mayo, M. S., and Cheung, H. C. *J. Biol. Chem.,* **271,** 9473–9482 (1996)
10. Ma, Y.-Z., and Taylor, E. W. (1997) *J. Biol. Chem.* **272,** 717–723
11. Sweeney, H. L., Rosenfeld, S. S., Brown, F., Faust, L., Smith, J., Xing, J., Stein, L., and Sellers, J. (1998) *J. Biol. Chem.* **273,** 6262–6270
12. Dong, W. J., Chandra, M., Xing, J., She, M., Solaro, R. J., and Cheung, H. C. (1997) *Biochemistry* **36,** 6754–6761
13. She, M., Dong, W.-J., Umeda, P. K., and Cheung, H. C. (1997) *Biophys. J.* **73,** 1042–1055
14. Straume, M., Frasier-Cadoret, S. G., and Johnson, M. L. (1991) in *Topics in Fluorescence Spectroscopy* (Lakowicz, J. R., ed) Vol. 2, pp. 177–239, Plenum Press, New York
15. Cheung, H. C., Wang, C.-K., Gryczynski, I., Wiczk, W., Laczko, G., Johnson, M. L., and Lakowicz, J. R. (1991) *Biochemistry* **30,** 5238–5247
16. Crevel, I. M., Lockhart, A., and Cross, R. A. (1996) *J. Mol. Biol.* **257,** 66–76
17. Stryer, L. (1978) *Annu. Rev. Biochem.* **47,** 819–846
18. Rosenfeld, S. S., Xing, J., Kar, S., Cheung, H. C., Brown, F., and Sweeney, H. L. (1998) *J. Biol. Chem.* **273,** 28682–28690
19. Ma, Y.-Z., and Taylor, E. W. (1995) *Biochemistry* **34,** 13233–13241
20. Gilbert, S. P., Webb, M. R., Brune, M., and Johnson, K. A. (1995) *Nature* **362,** 671–676
21. Gilbert, S. P., and Johnson, K. A. (1993) *Biochemistry* **32,** 4677–4684
22. Rosenfeld, S. S., and Taylor, E. W. (1984) *J. Biol. Chem.* **259,** 11920–11929
23. Ma, Y.-Z., and Taylor, E. W. (1997) *J. Biol. Chem.* **272,** 724–730
24. Gilbert, S. P., Moyer, M. L., and Johnson, K. A. (1998) *Biochemistry* **37,** 792–799
25. Hackney, D. D. (1994) *Proc. Natl. Acad. Sci. U. S. A.* **91,** 6865–6869
26. Moyer, M. L., Gilbert, S. P., and Johnson, K. A. (1998) *Biochemistry* **37,** 800–813
27. Hancock, W. O., and Howard, J. (1999) *Proc. Natl. Acad. Sci. U. S. A.* **96,** 13147–13152
28. Deleted in proof
29. Wriggers, W., and Schulten, K. (1998) *Biophys. J.* **75,** 646–661
30. Sablin, E. P., Kull, F. J., Cooke, R., Vale, R. D., and Fletterick, R. J. (1996) *Nature* **380,** 550–559
31. Gullick, A. M., Song, H., Endow, S. A., and Rayment, I. (1998) *Biochemistry* **37,** 1769
32. Vale, R. D., and Milligan, R. A. (2000) *Science* **288,** 88–95
33. Deleted in proof
34. Brendza, K. M., Rose, D. J., Gilbert, S. P., and Saxton, W. M. (1999) *J. Biol. Chem.* **274,** 31506–31514
35. Woehlke, G., Ruby, A. K., Hart, C. L., Ly, B., Hom-Boother, N., and Vale, R. D. (1997) *Cell* **90,** 207–216
36. Brünger, A. T. (1992) *X-PLOR, Version 3: A System for X-ray Crystallography and NMR*, Howard Hughes Medical Institute and Department of Molecular Biophysics and Biochemistry, Yale University, New Haven, CT
37. Brooks, B. R., Bruccoleri, R. E., Olafson, B. D., States, D. J., Swaminathan, S., and Karplus, M. (1983) *J. Comp. Chem.* **4,** 187–217
38. Pastor, R. W. (1994) in *The Molecular Dynamics of Liquid Crystals* (Luckhurst, G. R., and Veracini, C. A., eds) pp. 85–138, Kluwer Academic, Amsterdam, The Netherlands
39. Navone, F., Niclas, J., Hom-Booher, N., Sparks, L., Bernstein, H. D., McCaffery, G., and Vale, R. D. (1992) *J. Cell Biol.* **117,** 1263–1276